

## Dispersion due to wall interactions in microfluidic separation systems

Subhra Datta<sup>a)</sup> and Sandip Ghosal

*Department of Mechanical Engineering, Northwestern University,  
2145 Sheridan Road, Evanston, Illinois 60208, USA*

(Received 4 June 2007; accepted 1 November 2007; published online 29 January 2008)

The transport of a solute in a straight microchannel of axially variable cross-sectional shape in the presence of an inhomogeneous flow field and an adsorption-desorption process on the wall is studied, motivated by applications to capillary electrophoresis and open-channel capillary electrochromatography. An asymptotic approach based on the long time limit is adopted that reduces the problem to the solution of a one-dimensional transport equation. The reduced model is integrated numerically to study the effects of inhomogeneous electro-osmotic flow and adsorption-desorption kinetics on solute migration and dispersion in a rectangular microchannel. The accuracy of the asymptotic equations is checked by the direct numerical solution of the original three-dimensional transport problem. © 2008 American Institute of Physics. [DOI: 10.1063/1.2828098]

### I. INTRODUCTION

The problem of transport of a solute that can interact with channel walls is encountered very often in microfluidic chemical analysis techniques such as capillary electrophoresis (CE) and open-channel capillary electrochromatography (CEC).<sup>1,2</sup> In the latter, the interaction of a solute with a coating bonded to the channel wall serves as the separation principle;<sup>3,4</sup> in the former, it is often an undesirable effect.<sup>5–7</sup> In both techniques, electro-osmotic flow (EOF) is commonly employed to transport both the solvent and the solute in the microfluidic channels. The EOF is generated by externally applied electric fields that can act on the net charges present near a liquid-solid interface.<sup>8</sup> In this paper, we study the transport of a solute in inhomogeneous flows in the presence of adsorption and desorption on the wall, motivated by applications in CE and CEC under EOF.

The thickness of the diffuse charge layer at a liquid-solid interface is characterized by the Debye length  $\lambda_D$ , which is of the order of 1–10 nm for most solvents used in CE and CEC at room temperature.<sup>8</sup> If the width of a channel is much larger than  $\lambda_D$  and all properties are uniform, the EOF in the channel is to a good approximation a “plug flow” or uniform flow.<sup>8</sup> However, there are situations when the EOF is axially and radially inhomogeneous, for example, as a consequence of the variation of zeta potential and microchannel cross section,<sup>9</sup> or due to finite Debye layer effects.<sup>10</sup> While an inert solute in a uniform “plug” flow spreads solely on account of molecular diffusion, the presence of inhomogeneities in the flow leads to enhanced spreading of solute bands by the Taylor-Aris dispersion mechanism.<sup>11,12</sup> The effective diffusivity is inversely proportional to the molecular diffusivity of the solute in the analysis medium, and, for pressure-driven flow, is more significant at higher flow rates.<sup>11</sup> The analysis in this article is motivated by the problem of solute transport under nonideal electro-osmosis conditions in microfluidic devices.<sup>13</sup> However, it is more general in scope as it can account for any axially variable flow and cross-sectional shape changes,<sup>14,15</sup> provided they take place on a slow time and spatial scale in the axial direction.

Owing to the large surface to volume ratio of microfluidic channels, solute adsorption and desorption on channel walls is often a source of undesirable consequences like loss of sample<sup>16,17</sup> and loss of resolution<sup>2</sup> in techniques like CE and CEC. Specific studies relevant to modeling band broadening in CEC include Ref. 4 and Refs. 18–21. For studies relevant to CE, see e.g., Refs. 7 and 22, the reviews Ref. 9 and Ref. 23, and the references therein. When both adsorption and desorption are fast enough compared to the analysis time, the wall interactions can be characterized by the theory of chromatography.<sup>24–26</sup> Wall retention in chromatographic techniques, besides serving as the principle of separation<sup>25</sup> is also in itself a source of enhanced dispersion.<sup>24,27</sup> Dispersion due to retention and Taylor-Aris dispersion are coupled together in most modes of chromatography that employ inhomogeneous flow [e.g., gas chromatography<sup>28</sup> (GC) and liquid chromatography<sup>29</sup> (LC)].

We provide here a generalized treatment of an arbitrary wall reaction kinetic function. Unlike most theories of chromatography,<sup>25</sup> the analysis does not require that the departures from a state of “chemical equilibrium” to be small. Consequently, it can be used to study dispersion at much shorter times from the start of chemical analysis than available chromatography theories and is also applicable for slower and nearly irreversible adsorption processes encountered in proteomic applications of CE.<sup>16,30</sup> In the special case of fast linear kinetics, the analysis reaffirms known results from the theory of chromatography<sup>25</sup> and can also predict chromatographic dispersion in complex microfluidic cross-sectional shapes like rectangle and trapezoid under various flow conditions, such as, electrokinetic flow with finite Debye layers,<sup>31</sup> pressure-driven flow,<sup>25</sup> the shear flow used to transport solutes in shear-driven chromatography,<sup>32</sup> and electro-osmotic micropump driven circular chromatography.<sup>33</sup> The analysis also resolves the three-dimensional distribution of the solute in the microchannel, a feature that is absent in analyses based on method of moments<sup>26</sup> or its generalizations.<sup>34</sup> There are previous works that provide asymptotic approximations for the concentration

field as well as area averaged concentration in a channel,<sup>35–37</sup> but none of them treat simultaneously inhomogeneous flows, arbitrary cross sections, and arbitrary wall kinetics, like the present work.

Owing to the small width to length ratio of microchannels, direct numerical solution of the three-dimensional transport problem for the concentration  $c$  of the solute in the microchannel is expensive and gives rise to a “stiff system.”<sup>38</sup> We use an asymptotic theory to obtain a formulation that requires only the solution of one-dimensional partial differential equations for the area averaged concentration of the solute  $\bar{c}$ . The concentration distribution  $c$  can be calculated explicitly in terms of  $\bar{c}$  and its spatial derivative in the axial direction. Thus, complete information of the concentration distribution in three dimensions may be obtained at only a fraction of the computational cost involved in direct numerical simulation of the full transport problem.

The asymptotic theory presented in this paper generalizes the theoretical development in Ref. 7 which is applicable to axisymmetric cylindrical capillaries of constant cross section. In its present form, the analysis can account for arbitrary cross-sectional shapes and a slow axial variation in cross section. The solution starting from arbitrary initial conditions is accurate, except possibly during a short transient phase of duration of the order of the cross-channel diffusion time. As in Ref. 7 the form of the wall reaction kinetics is left arbitrary, but unlike Ref. 7, transverse as well as axial variation of unadsorbed and adsorbed solute on the wall is admitted. The requirement of “slow reactions” in Ref. 7 is relaxed thereby extending the applicability of the theory to chromatographic techniques, in addition to CE.

Several specific examples of the asymptotic theory will be discussed, all involving transport of the solute in rectangular microchannels.<sup>39,40</sup> These problems will be studied simultaneously with both three-dimensional direct numerical simulation and the asymptotically reduced equations, in order to check the accuracy of the asymptotic approach.

In Sec. II, we develop the asymptotic theory for dispersion in axially variable flows and geometries with arbitrary wall reaction kinetics. In Sec. III, we consider the special case of linear adsorption/desorption kinetics and further study an interesting limit encountered in chromatography when both adsorption and desorption processes are nearly at equilibrium. We also describe the procedure to specialize our model to specific flow types and geometries in this section. In Sec. IV, we solve the three-dimensional equations governing transport and adsorption-desorption in a rectangular microchannel numerically and compare the results with those from the solution of the asymptotically reduced model. We present our main conclusions in Sec. V.

## II. ASYMPTOTIC EQUATIONS FOR SLOW AXIAL VARIATION

Consider a straight channel with arbitrarily varying cross section and wall charge (Fig. 1) in which there is an incompressible flow  $\mathbf{u}(x, y, z, t)$ , where  $x, y, z$  are coordinates relative to an orthogonal coordinate system with the  $x$ -axis along the axis of the channel. At any point on the wall of the

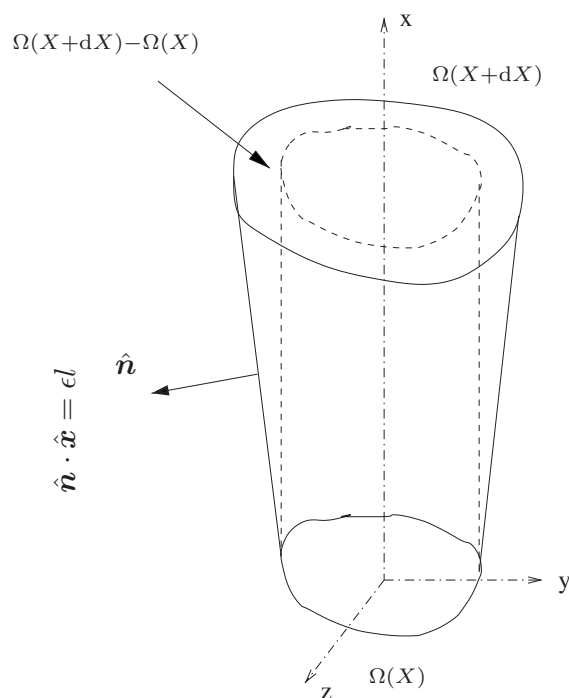


FIG. 1. Channel of axially variable cross section.

channel, the surface normal is given by  $\hat{\mathbf{n}}$ . The channel carries a solute of concentration  $c(x, y, z, t)$  moles per unit volume, some of which is adsorbed to the wall, which has a wall concentration  $s(x, y, z, t)$  moles per unit area. We choose a characteristic channel width  $w_0$  as our unit of length and  $w_0/u_e$  as our unit of time where  $u_e$  is a characteristic flow speed. We assume that the concentration  $c$  has been normalized by some characteristic value  $c^*$  and the wall concentration  $s$  by  $c^* w_0$ . The Peclet number is  $\text{Pe} = (u_e w_0)/D$ , where  $D$  is the solute diffusivity. Then the following equations describe the time evolution of the  $c(x, y, z, t)$ ,

$$c_t + \mathbf{u} \cdot \nabla c = \text{Pe}^{-1} \nabla^2 c, \quad (1a)$$

$$\text{Pe}^{-1} \nabla c \cdot \hat{\mathbf{n}} = -s_t \text{ on wall.} \quad (1b)$$

As shown in Fig. 1, the cross section of the channel at each axial location  $x$  is denoted by the two-dimensional domain  $\Omega(x)$  bounded by the curve  $\partial\Omega(x)$ . The normal to  $\partial\Omega$  is  $\hat{\mathbf{n}}_\Omega$ .

### A. Slow variations

We suppose that a time much larger than the diffusion time across the channel (i.e.,  $t \gg \text{Pe}$ ) has elapsed so that any axial variation takes place on a long length scale and a slow time scale. We define the scaled “slow variables”  $X = \epsilon x$  and  $T = \epsilon t$ . In order to ensure slow variation, any dependence of the flow  $\mathbf{u}(x, y, z, t)$  on  $x$  and  $t$  has to be slow and the cross section of the microchannel should change slowly in the axial direction. The latter requirement means the surface normal  $\hat{\mathbf{n}}$  at any point on the wall makes a small angle with the  $x$ -axis, or in other words,

$$\hat{\mathbf{n}} = \epsilon \hat{\mathbf{x}} + \sqrt{1 - \epsilon^2 l^2} \hat{\mathbf{n}}_\Omega, \quad (2)$$

where  $\hat{\mathbf{n}}_\Omega$  is the unit normal at the boundary  $\partial\Omega(X)$  of the 2D domain  $\Omega(x)$ .<sup>41</sup> If the axial velocity  $u$  is  $O(1)$  from the requirements of continuity of flow, the cross flow velocity components  $v$  and  $w$  must be  $O(\epsilon)$ . So, we write,  $\mathbf{u} = U\hat{\mathbf{x}} + v\hat{\mathbf{y}} + w\hat{\mathbf{z}} = U\hat{\mathbf{x}} + \epsilon\mathbf{U}_\perp$  and construct the following asymptotic expansion for the velocity field:

$$u = U(X, y, z, T; \epsilon) = U^{(0)} + \epsilon U^{(1)} + \dots, \quad (3a)$$

$$v\hat{\mathbf{y}} + w\hat{\mathbf{z}} = \epsilon\mathbf{U}_\perp = \epsilon\mathbf{U}_\perp^{(0)} + \epsilon^2\mathbf{U}_\perp^{(1)} + \dots. \quad (3b)$$

Changing variables from  $x$  and  $t$  to  $X$  and  $T$ , Eq. (1) becomes

$$\epsilon c_T + \epsilon U c_X + \epsilon\mathbf{U}_\perp \cdot \nabla_\Omega c - \epsilon^2 \text{Pe}^{-1} c_{XX} = \text{Pe}^{-1} \nabla_\Omega^2 c, \quad (4a)$$

$$\text{Pe}^{-1} (\sqrt{1 - \epsilon^2 l^2} \nabla_\Omega c \cdot \hat{\mathbf{n}}_\Omega + \epsilon^2 l c_X)|_{\partial\Omega} = -\epsilon s_T, \quad (4b)$$

where  $\nabla_\Omega$  is the two-dimensional gradient operator in the domain  $\Omega$ . The variables  $c$  and  $s$  can be expanded in powers of  $\epsilon$ ,

$$c = c^{(0)} + \epsilon c^{(1)} + \dots, \quad (5a)$$

$$s = s^{(0)} + \epsilon s^{(1)} + \dots \quad (5b)$$

and substituted in Eqs. (4a) and (4b). Equating coefficients of like powers of  $\epsilon$  we get a succession of boundary value problems, which we consider next.

## B. Order $\epsilon^0$

At  $O(1)$  we have

$$\text{Pe}^{-1} \nabla_\Omega^2 c^{(0)} = 0, \quad (6a)$$

$$-\text{Pe}^{-1} \nabla_\Omega c^{(0)} \cdot \hat{\mathbf{n}}_\Omega|_{\partial\Omega} = 0. \quad (6b)$$

This implies that  $c^{(0)}$  is independent of the cross-sectional coordinates  $y$  and  $z$ , that is,  $c^{(0)} = \bar{c}^{(0)}(X, T)$ . A bar over a quantity indicates an average defined at each axial location  $X$  and time  $T$ : for quantities defined within the channel (e.g.,  $c$ ) the average is over the two-dimensional region  $\Omega(X)$ , for quantities defined on the wall of the channel (e.g.,  $s$ ) the average is over the one-dimensional bounding curve  $\partial\Omega(X)$ . Equations (6a) and (6b) however, do not determine  $c^{(0)}$  uniquely because it is satisfied by any function  $\bar{c}^{(0)}(X, T)$  of  $X$  and  $T$ . To determine this function, we must now consider the boundary value problem at the next order.

## C. Order $\epsilon$

At  $O(\epsilon)$  we have

$$\text{Pe}^{-1} \nabla_\Omega^2 c^{(1)} = \bar{c}_T^{(0)} + U^{(0)} \bar{c}_X^{(0)}, \quad (7a)$$

$$-\text{Pe}^{-1} \nabla_\Omega c^{(1)} \cdot \hat{\mathbf{n}}_\Omega|_{\partial\Omega} = s_T^{(0)}. \quad (7b)$$

### 1. Solvability condition

Equations (7a) and (7b) have no solutions unless a solvability condition is satisfied by the lower order solution. Integrating both sides of Eq. (7a) in the region  $\Omega(X)$ ,

$$\int \text{Pe}^{-1} \nabla_\Omega^2 c^{(1)} dA = A \bar{c}_T^{(0)} + A \bar{U}^{(0)} \bar{c}_X^{(0)}. \quad (8)$$

Using the two-dimensional Gauss Divergence Theorem the area integral on  $\Omega(X)$  is converted to a line integral along the curve  $\partial\Omega(X)$ . Thus,

$$\begin{aligned} & \oint \text{Pe}^{-1} \nabla_\Omega c^{(1)} \cdot \hat{\mathbf{n}}_\Omega dS \\ &= \int \text{Pe}^{-1} \nabla_\Omega^2 c^{(1)} dA = A \bar{c}_T^{(0)} + A \bar{U}^{(0)} \bar{c}_X^{(0)} \end{aligned} \quad (9)$$

( $dA$  and  $dS$  denote the differential area element and arc length). Finally, using Eq. (7b) in the integrand on the left-hand side of the equality and rearranging, we get

$$\bar{c}_T^{(0)} + \bar{U}^{(0)} \bar{c}_X^{(0)} = -\alpha \bar{s}_T^{(0)}, \quad (10)$$

where  $\alpha(X)$  is defined as the ratio of the perimeter  $\Gamma$  (measured in  $w_0$  units) and dimensionless area  $A$  (measured in  $w_0^2$  units) of the cross section at any  $X$ .

## 2. Solution for $\bar{c}^{(1)}$

Equation (10) is a necessary condition for nontrivial solutions of Eqs. (7a) and (7b) to exist. If it is satisfied, then we may proceed to the next step, which is, determining the structure of this solution. First, Eq. (10) can be used to rewrite Eq. (7) as follows:

$$\text{Pe}^{-1} \nabla_\Omega^2 c^{(1)} = -\alpha \bar{s}_T^{(0)} + [U^{(0)} - \bar{U}^{(0)}] \bar{c}_X^{(0)}, \quad (11a)$$

$$-\text{Pe}^{-1} \nabla_\Omega c^{(1)} \cdot \hat{\mathbf{n}}_\Omega|_{\partial\Omega} = s_T^{(0)}. \quad (11b)$$

Solutions to Eq. (11a) satisfying the boundary condition in Eq. (11b) may in general be written as

$$c^{(1)} = \bar{c}^{(1)} + \text{Pe}[-\alpha \bar{s}_T^{(0)} f^{(0)} + \bar{U}^{(0)} \bar{c}_X^{(0)} g^{(0)}]. \quad (12)$$

Here,  $f^{(0)}$  is defined by the following boundary value problem:

$$\nabla_\Omega^2 f^{(0)} = 1, \quad (13a)$$

$$\nabla_\Omega f^{(0)} \cdot \hat{\mathbf{n}}_\Omega = \frac{1}{\alpha} \frac{s_T^{(0)}}{\bar{s}_T^{(0)}}, \quad (13b)$$

$$\bar{f}^{(0)} = 0. \quad (13c)$$

Equation (13c) is imposed in order to eliminate the arbitrariness of  $f^{(0)}$  up to a constant. Similarly,  $g^{(0)}$  is defined by the boundary value problem,

$$\nabla_\Omega^2 g^{(0)} = \frac{U^{(0)}}{\bar{U}^{(0)}} - 1, \quad (14a)$$

$$\nabla_\Omega g^{(0)} \cdot \hat{\mathbf{n}}_\Omega|_{\partial\Omega} = 0, \quad (14b)$$

$$\bar{g}^{(0)} = 0. \quad (14c)$$

## D. Order $\epsilon^2$

At order  $O(\epsilon^2)$  we have

$$\text{Pe}^{-1} \nabla_{\Omega}^2 c^{(2)} = c_T^{(1)} + U^{(0)} c_X^{(1)} + U^{(1)} \bar{c}_X^{(0)} + \mathbf{U}_{\perp}^{(0)} \cdot \nabla_{\Omega} c^{(1)} - \text{Pe}^{-1} \bar{c}_{XX}^{(0)}, \quad (15a)$$

$$- \text{Pe}^{-1} \nabla_{\Omega} c^{(2)} \cdot \hat{\mathbf{n}}_{\Omega}|_{\partial\Omega} = s_T^{(1)} + \text{Pe}^{-1} l \bar{c}_X^{(0)}. \quad (15b)$$

### 1. Solvability condition

Integrating both sides of Eq. (15a) over the region  $\Omega(X)$  as before, we derive

$$-\bar{s}_T^{(1)} \Gamma = -\text{Pe}^{-1} \left[ A \bar{c}_{XX}^{(0)} - \bar{c}_X^{(0)} \oint_{\partial\Omega} l dS \right] + \left[ \int_{\Omega} U^{(0)} c_X^{(1)} dA + \int_{\Omega} \mathbf{U}_{\perp}^{(0)} \cdot \nabla_{\Omega} c^{(1)} dA \right] + A \bar{U}_1 \bar{c}_X^{(0)} + A \bar{c}_T^{(1)}. \quad (16)$$

The terms enclosed in brackets in Eq. (16) can be simplified using the geometrical result (see Appendix A),

$$\left( \int_{\Omega} F dA \right)_X = \int_{\Omega} F_X dA - \oint_{\partial\Omega} F l dS, \quad (17)$$

the equation of continuity,  $U_X + \nabla \cdot \mathbf{U}_{\perp} = 0$  and the condition of no flow through the wall,  $\mathbf{u} \cdot \hat{\mathbf{n}} = 0$ .

The terms enclosed in brackets in Eq. (16) become

$$A \bar{c}_{XX}^{(0)} - \bar{c}_X^{(0)} \oint_{\partial\Omega} l dS = [A \bar{c}_X^{(0)}]_X, \quad (18a)$$

$$\int_{\Omega} U^{(0)} c_X^{(1)} dA + \int_{\Omega} \mathbf{U}_{\perp}^{(0)} \cdot \nabla_{\Omega} c^{(1)} dA = [A \overline{c^{(1)} U^{(0)}}]_X. \quad (18b)$$

Substituting this in Eq. (16) we get the following solvability condition for the problem at  $O(\epsilon^2)$ :

$$-\alpha A \bar{s}_T^{(1)} = -\text{Pe}^{-1} (A \bar{c}_X^{(0)})_X + (A \overline{c^{(1)} U^{(0)}})_X + A \bar{U}_1 \bar{c}_X^{(0)} + A \bar{c}_T^{(1)}. \quad (19)$$

### E. Reconstitution

We can obtain a single equation for  $c = c^{(0)} + \epsilon c^{(1)} + O(\epsilon^2)$  by combining Eqs. (10) and (19): adding  $A$  times Eq. (10), with  $\epsilon$  times Eq. (19) and inserting the  $O(\epsilon^2)$  terms  $\epsilon^2 [A \overline{c^{(1)} U^{(1)}}]_X$  and  $-\epsilon^2 \text{Pe}^{-1} [A \bar{c}_X^{(1)}]_X$  [doing so does not affect the asymptotic validity of the resultant equation up to  $O(\epsilon)$ ] we get

$$-\alpha A (\bar{s}_0 + \epsilon \bar{s}_1)_T = -\epsilon \text{Pe}^{-1} \{ A [\bar{c}^{(0)} + \epsilon \bar{c}^{(1)}]_X \}_X + \{ A [\overline{c^{(0)} + \epsilon c^{(1)}}] (U_0 + \epsilon U_1) \}_X + A [\bar{c}^{(0)} + \epsilon \bar{c}^{(1)}]_T + O(\epsilon^2). \quad (20)$$

To get the form of the second term on the right-hand side of Eq. (20) we have made use of the fact that the velocity field  $\mathbf{u}$  is solenoidal, so that

$$(\bar{U}A)_X = \{ A [\bar{U}^{(0)} + \epsilon \bar{U}^{(1)} + \epsilon^2 \bar{U}^{(2)} + \dots] \}_X = 0. \quad (21)$$

Finally, reverting back to independent variables  $t = T/\epsilon$  and  $x = X/\epsilon$  and substituting  $c = c^{(0)} + \epsilon c^{(1)} + O(\epsilon^2)$  and  $s = s^{(0)} + \epsilon s^{(1)} + O(\epsilon^2)$ ,

$$-\alpha A \bar{s}_t = -\text{Pe}^{-1} (A \bar{c}_x)_x + (A \overline{c u})_x + A \bar{c}_t \quad (22)$$

with an error of  $O(\epsilon^2)$ . Combining  $c^{(0)} = \bar{c}^{(0)}$  and Eq. (12) and reverting to  $t$  and  $x$ ,

$$c = \bar{c} + \text{Pe}(-\alpha \bar{s}_t f + \bar{u} \bar{c}_x g), \quad (23)$$

where  $f = f^{(0)} + O(\epsilon)$  and  $g = g^{(0)} + O(\epsilon)$  are calculated by modifying the boundary value problems in Eqs. (13) and (14),

$$\nabla_{\Omega}^2 f = 1, \quad (24a)$$

$$\nabla_{\Omega} f \cdot \hat{\mathbf{n}}_{\Omega}|_{\partial\Omega} = \frac{1}{\alpha} \frac{s_t}{\bar{s}_t}, \quad (24b)$$

$$\bar{f} = 0, \quad (24c)$$

$$\nabla_{\Omega}^2 g = \frac{u}{\bar{u}} - 1, \quad (25a)$$

$$\nabla_{\Omega} g \cdot \hat{\mathbf{n}}_{\Omega}|_{\partial\Omega} = 0, \quad (25b)$$

$$\bar{g} = 0. \quad (25c)$$

Equation (23) can be substituted in Eq. (22). Defining the coefficients  $\beta$  and  $\gamma$  by

$$\beta \bar{u} = -\bar{f} u, \quad (26a)$$

$$\gamma \bar{u} = -\bar{g} u \quad (26b)$$

we get

$$A \bar{c}_t + (A \bar{u} \bar{c})_x = -\alpha A \bar{s}_t + (A D^* \bar{c}_x)_x - \text{Pe}(\alpha A \beta \bar{u} \bar{s}_t)_x, \quad (27a)$$

$$D^* = \text{Pe}^{-1} + \gamma \text{Pe} \bar{u}^2. \quad (27b)$$

Equations (23) and (27) are our asymptotic equations for determining  $c$ . They have an error of  $O(\epsilon^3)$  or higher.

### III. APPLICATIONS

The surface concentration must be specified by a kinetic law of the following form:

$$s_t = h(c_w, s, \dots), \quad (28)$$

where  $c_w$  denotes the solute concentration on the wall and the  $\dots$  indicate parameters (such as kinetic coefficients) that may or may not have a space time dependence. The function  $h$  in Eq. (28) can be expanded in Taylor series around  $\bar{c}$  using Eq. (23),

$$s_t = h(\bar{c}, s, \dots) + h_{c_w}|_{c_w=\bar{c}} \text{Pe}(-\alpha \bar{s}_t f_w + \bar{u} \bar{c}_x g_w) + O(\epsilon^2). \quad (29)$$

Here,  $f_w$  and  $g_w$  stand for the value of the functions  $f$  and  $g$  on the wall and  $h_{c_w}|_{c_w=\bar{c}}$  indicates partial derivative of  $h$  with respect to  $c_w$  evaluated at  $c_w = \bar{c}$ .

### A. Linear kinetics with constant coefficients

A linear reaction law of the form,

$$s_t = h(c_w, s, \lambda, K) = \lambda(Kc_w - s) \quad (30)$$

will now be specified, where  $\lambda$  is the rate constant of desorption from the wall and  $K$  is the equilibrium constant of the adsorption-desorption process. The combination  $\lambda K$  is the rate constant of adsorption. For such linear kinetics,  $h_{c_w}|_{c_w=\bar{c}} = \lambda K$ . Averaging Eq. (29) specialized to linear kinetics along the bounding curve  $\partial\Omega(x)$  and rearranging,

$$(1 + \alpha \lambda K \text{Pe} \bar{f}_w) \bar{s}_t + \lambda \bar{s} = \lambda K (\bar{c} + \text{Pe} \bar{u} \bar{c}_x \bar{g}_w) + O(\epsilon^2). \quad (31)$$

Here, it has been assumed that  $\lambda$  and  $K$  do not vary along the curve  $\partial\Omega(x)$ . The notation  $\bar{f}_w$  and  $\bar{g}_w$  indicate  $f_w$  and  $g_w$  averaged over  $\partial\Omega(x)$ . The asymptotically reduced equations [Eqs. (27) and (31)] can be solved simultaneously to find an asymptotic approximation to the axial distribution of  $\bar{c}$ . The three-dimensional distribution of  $c$  can be calculated from the axial distribution of  $\bar{c}$ , using Eq. (23).

### B. The limit of fast reactions

Further analytical simplification of Eq. (27) is possible when reactions at the wall happen on a time scale that is short compared to the analysis time. Thus, adsorption and desorption are nearly in equilibrium over most of the time interval over which knowledge of the analyte concentration is of interest. The scaling that best describes this situation is  $\lambda \sim K \sim O(1)$ . In order to get a simple result, we further assume that the flow is homogeneous in the axial direction and the cross section of the channel does not vary in shape or area in the axial direction. Under these conditions  $A$ ,  $\alpha$ ,  $\beta$ , and  $\gamma$  are independent of  $x$  and  $t$  and  $\bar{u}$  is a constant. So, Eq. (27) can be rewritten as

$$\bar{c}_t + \bar{u} \bar{c}_x = -\alpha \bar{s}_t + [(\text{Pe}^{-1} + \gamma \text{Pe} \bar{u}^2) \bar{c}_x]_x - \text{Pe} \alpha \beta \bar{u} \bar{s}_{tx} \quad (32)$$

with an error of  $O(\epsilon^3)$ . In the long time limit,  $t \sim 1/\epsilon$ , the order of magnitude of the terms in Eq. (31) can be estimated as follows: the second term on the left-hand side of the equality and the first term on the right-hand side of the equality are both  $O(1)$  and the remaining terms are  $O(\epsilon)$  or less. So, the leading order balance in Eq. (31) may be written as

$$\bar{s} = K \bar{c} + O(\epsilon). \quad (33)$$

We note that from Eq. (27) at leading order

$$\bar{c}_t + \bar{u} \bar{c}_x = -\alpha \bar{s}_t + O(\epsilon^2). \quad (34)$$

Using Eq. (33) in Eq. (34), we get

$$\bar{c}_t = -\frac{\bar{u}}{1 + \alpha K} \bar{c}_x + O(\epsilon^2). \quad (35)$$

Differentiation of Eq. (33) with respect to  $t$  leads to  $\bar{s}_t = K \bar{c}_t + O(\epsilon^2)$  in the long time limit, this can be used to replace the terms with  $\bar{s}_t$  in Eq. (31) without the loss of asymptotic accuracy. On rearrangement of the resultant expression, we get

$$\bar{s} = K \bar{c} - \left( \frac{K}{\lambda} + \text{Pe} \alpha K^2 \bar{f}_w \right) \bar{c}_t + K \text{Pe} \bar{g}_w \bar{u} \bar{c}_x + O(\epsilon^2). \quad (36)$$

Using Eq. (35) in Eq. (36) we get

$$\bar{s} = K \bar{c} + \bar{u} \bar{c}_x \left[ \left( \frac{K}{\lambda(1 + \alpha K)} + \text{Pe} \frac{\alpha K^2 \bar{f}_w}{1 + \alpha K} \right) + K \text{Pe} \bar{g}_w \right] + O(\epsilon^2). \quad (37)$$

Differentiating Eq. (37) with respect to  $t$  and noting that  $\bar{c}_{xt} = \bar{c}_{tx}$  can be calculated by differentiation of Eq. (35) with respect to  $x$  we get

$$\bar{s}_t = K \bar{c}_t - \left\{ \frac{K}{\lambda(1 + \alpha K)^2} + \left[ \frac{\alpha K^2 \bar{f}_w}{(1 + \alpha K)^2} + \frac{K \bar{g}_w}{(1 + \alpha K)} \right] \text{Pe} \right\} \bar{u}^2 \bar{c}_{xx} + O(\epsilon^3). \quad (38)$$

The  $\bar{s}_t$  calculated by Eq. (38) can be used in Eq. (32) to arrive at the effective equation in the limit of fast reactions. Since the last term  $-\text{Pe} \alpha \beta \bar{u} \bar{s}_{tx}$  of Eq. (32) is of the order of  $O(\epsilon^2)$ , it is sufficient to use an  $O(\epsilon)$  accurate approximation of Eq. (38) in approximating this term,

$$\bar{s}_t = K \bar{c}_t + O(\epsilon^2) = -\frac{K}{1 + \alpha K} \bar{u} \bar{c}_x + O(\epsilon^2), \quad (39)$$

where Eq. (35) has been used to obtain the second equality. The first term  $-\alpha \bar{s}_t$  on the right-hand side of Eq. (32) is  $O(\epsilon)$ , so in approximating it by Eq. (38), all terms of Eq. (38) have to be retained. After this substitution to Eq. (38), we get on rearrangement,

$$\bar{c}_t + \frac{\bar{u}}{1 + K'} \bar{c}_x = D_{\text{eff}} \bar{c}_{xx}, \quad (40)$$

where  $K' = \alpha K$  and

$$D_{\text{eff}} = D_{\text{eff}}^{(\text{chrom})} = \frac{\text{Pe}^{-1}}{1 + K'} + \left[ \frac{\gamma}{1 + K'} + \frac{2K' \beta}{(1 + K')^2} + \frac{K'^2 \bar{f}_w}{(1 + K')^3} \right] \text{Pe} \bar{u}^2 + \frac{K'}{\lambda(1 + K')^3} \bar{u}^2. \quad (41)$$

In the above  $\bar{g}_w = \beta$  has been used. A proof of this is presented in Appendix B.

In the analysis presented in this section, we assumed the scalings  $\lambda \sim \lambda K \sim 1$ . If the adsorption and desorption reactions are even faster, that is, chemical equilibrium is established on a time scale much shorter than the cross channel transport time, then  $\lambda \sim \lambda K \sim 1/\epsilon$  is an appropriate scaling. If the analysis presented in this section is repeated using  $\lambda = \bar{\lambda}/\epsilon$ , where  $\bar{\lambda}$  is independent of  $\epsilon$ , then it is easily verified

that one recovers Eqs. (40) and (41), except for the last term in Eq. (41) which drops out. One could also arrive at Eqs. (40) and (41) by reversing the two limiting procedures, that is, invoking the “quasiequilibrium” assumption before the asymptotic analysis describing the Taylor regime as in the work of Golay<sup>24</sup> and others. The other possibilities involving fast reactions are (A)  $\lambda K \sim 1/\epsilon$  and  $\lambda \sim 1$ ; (B)  $\lambda K \sim 1$  and  $\lambda \sim 1/\epsilon$ . In case (A) almost all of the analyte is adsorbed in the first few capillary diameters and in case (B) retention is negligible. In both cases though, Eq. (41) correctly describes the appropriate limiting situation.

### C. Shape functions in different flows and geometries

In order to proceed further with the asymptotically reduced problem, it is essential to calculate the shape functions  $f$  and  $g$ . This enables us to calculate the quantities  $\beta$ ,  $\gamma$ , and  $\bar{f}_w$  appearing in the equations derived so far for  $\bar{c}$  and  $\bar{s}$  and also to find the concentration variation across a given cross section through Eq. (23).

The function  $f$  calculated by solving Eq. (24) depends only on the geometry of the channel if the kinetic coefficients of adsorption-desorption and initial conditions on  $s$  are the same for all points on the curve  $\partial\Omega$  and can be calculated by solving Eq. (24) with the right-hand side of Eq. (24b) set to  $1/\alpha$  (see Appendix B). Planar, rectangular, and trapezoidal microchannels are some common shapes of interest.<sup>40</sup>

The function  $g$  calculated by solving Eq. (25) depends both on the type of flow and geometry. Some interesting and useful flows for which the function  $g$  and the coefficients  $\gamma$  and  $\beta$  are relevant are

- (i) Purely pressure-driven flow employed in liquid and gas chromatography<sup>25</sup> and used for theoretical modeling of axially variable electro-osmotic flow.<sup>42</sup>
- (ii) Shear-driven (Couette) flow for novel techniques such as chromatography with electro-osmotic micropumping<sup>33</sup> and shear-driven chromatography.<sup>32</sup>
- (iii) Electrokinetic flow with finite Debye layer effects (to be studied in Sec. IV under problem B).

All the above flow profiles are axially homogeneous, so the quantities  $\beta$  and  $\gamma$  are evaluated to be constant coefficients. In an axially inhomogeneous flow, like problem C, as shown later in Sec. IV, these quantities are a function of the axial coordinate  $x$ .

Table I shows the quantities  $\bar{f}_w$ ,  $\beta$ , and  $\gamma$  calculated for pressure-driven flow in channels with uniform kinetic coefficients of adsorption-desorption for some cross sections of interest in microfluidics (gap between planes, circle, square, and trapezoid). Except for the trapezoidal cross section for which  $f$  and  $g$  was obtained numerically, analytical solutions to Eqs. (24) and (25) can be readily calculated or obtained from the literature.<sup>36,43–45</sup> Table I will be referred to in solving the asymptotically reduced forms of the test problems in the next section. The information in Table I when used in Eq. (41) reaffirms classical results for the effective dispersion coefficient in chromatography with plane and round channels.<sup>24–26</sup>

TABLE I. The coefficients  $\bar{f}_w$ ,  $\beta$ , and  $\gamma$  calculated for an axially homogeneous and purely pressure-driven flow in a plane channel (gap between parallel plates) and in channels with circular, square, and trapezoidal cross section. The isosceles trapezoid in the last column is one for which the distance between the parallel sides equals half the sum of the parallel sides. The reference length-scale  $w_0$  is the diameter for the circle and the distance between the parallel sides for the other geometrical shapes.

Channel type	Plane	Circular	Square	Trapezoidal
$\bar{f}_w$	$\frac{1}{12}$	$\frac{1}{32}$	$\frac{1}{24}$	0.113
$\beta$	$\frac{1}{60}$	$\frac{1}{96}$	0.0155	0.052
$\gamma$	$\frac{1}{210}$	$\frac{1}{192}$	0.0084	0.0329

The gap between parallel planes can be used to approximate the microfluidic channels used in shear chromatography<sup>32</sup> and electro-osmotic micropumping.<sup>46</sup> The flow profile in either case is, then linear in the coordinate across the channel width. In this case, we obtain  $\bar{f}_w=1/3$ ,  $\beta=1/12$  and  $\gamma=1/30$  on solving Eqs. (24) and (25). While calculating  $f$ , care should be taken to account for the fact that shear chromatography and chromatography with electro-osmotic micropumping employ an adsorptive coating only on the passive (electrode-free<sup>32</sup> or stationary<sup>33</sup>) wall. Use of these values of  $\bar{f}_w$ ,  $\beta$ , and  $\gamma$  in Eq. (41) reaffirms the expression for effective dispersion coefficient derived in Ref. 32 using the Method of Moments.<sup>26</sup>

The shape function  $g$  for electrokinetic flows with finite Debye layers can be obtained numerically, given the analytical expression for the flow field.<sup>10</sup> Details of calculation of the coefficients  $\beta$  (when wall adsorption is present) and  $\gamma$  in this case will be presented in Sec. IV C.

## IV. NUMERICAL SIMULATIONS

A complete solution of the problem of transport generally involves solving Eq. (1) in three dimensions. The model developed in the last section requires solution of only one-dimensional equations. For the purpose of brevity, the former approach will be called the “three-dimensional model” and the latter approach will be called the “asymptotically reduced model.” In this section, three specific test problems will be solved numerically using both of these methods and the results compared to ascertain the accuracy of the asymptotic reduction.

### A. Test problems

The test problems pertain to transport of the solute under electro-osmotic flow. Additionally, the following specific conditions common to all the test problems to be described will be assumed:

- (i) The microchannel has an axially invariant square cross section of side  $2b$ . With the choice  $w_0=2b$ , the geometric constant  $\alpha=4$ .
- (ii) Wall reaction, when present, is of the linear form as described by Eq. (30) with  $\lambda$  and  $K$  invariant on the wall.

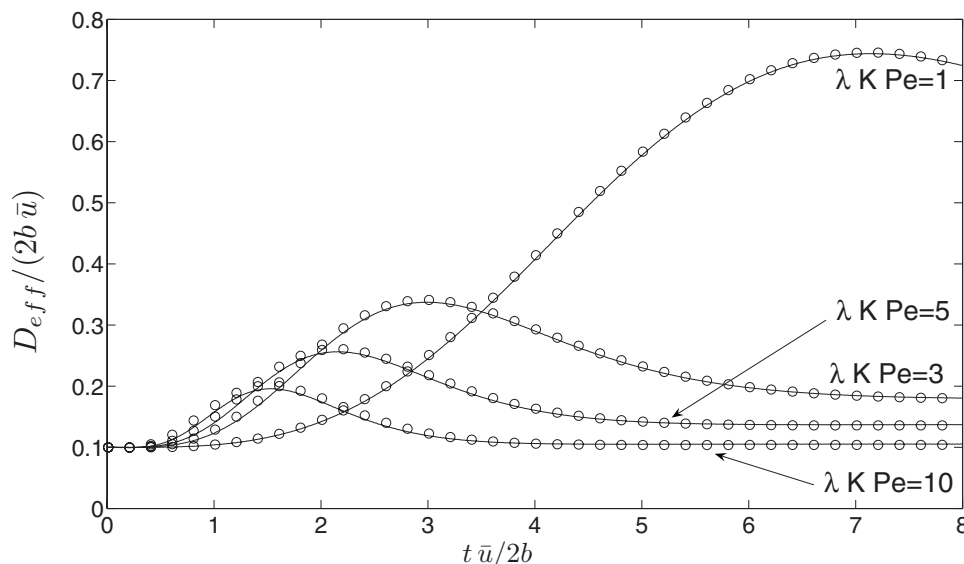


FIG. 2. Effective dispersion coefficient ( $D_{\text{eff}}$ ) vs time ( $t$ ) for  $\lambda K \text{Pe}=1, 3, 5, 10$  for problem A. The circular symbols represent results from three-dimensional numerical simulation and solid lines represent results from simulation of the asymptotically reduced model.

- (iii) Initially, there is no wall adsorbed concentration,  $s=0$  at  $t=0$ .
- (iv) The initial concentration of the solute  $c(x, y, z, t=0)$  is uniform across the channel and has a Gaussian distribution along the channel.
- (v) At any fixed axial location,  $x$ , the zeta potential does not vary over the bounding curve  $\partial\Omega(x)$ .

The velocity scale  $u_e$  for each test problem is chosen to ensure that the dimensionless speed  $\bar{u}$  is unity. We consider the following test problems:

**Problem A (EOF with wall reaction and infinitely thin Debye layers):** The solute is transported by a uniform plug flow with adsorption and desorption on the walls. In Eq. (30), the dimensionless equilibrium constant  $K$  will be held constant at the value  $K=1$  and  $\lambda$  will be varied to study the effect of varying wall reaction rates. This test problem is of relevance to separations by CEC,<sup>18</sup> as well as to the issue of band broadening due to wall-adsorption of charged species in CE.<sup>17</sup> The uniform flow profile arises in situations where the channel width is much larger than the Debye length and the wall properties are uniform. It also applies when the analyte is transported by electrophoresis alone in a channel where EOF has been suppressed. The Peclet number is  $\text{Pe}=10$  and the numerical domain size in the  $x$  direction is  $L/(2b)=40$ .

**Problem B (EOF with wall reaction and finite Debye layers):** Transport of a neutral solute in a channel with finite sized Debye layer will be analyzed, when an adsorption-desorption process ( $K=1$  and  $\lambda K \text{Pe}=1$ ) is present on the wall. The Debye layer thickness nondimensionalized by the width of the channel will be varied. The Peclet number is  $\text{Pe}=10$  and numerical domain size in the  $x$  direction is  $L/(2b)=40$ .

**Problem C (EOF with variable  $\zeta$  potential):** Dispersion under an axially varying EOF generated by a periodic zeta potential distribution  $\zeta = \zeta_0 + \Delta\zeta \cos(2\pi x/\Lambda)$  on all four walls of the square channel in absence of wall reactions will be

studied by varying  $\Lambda$  and  $\Delta\zeta$ . The Reynolds number of the flow is zero, the Peclet number is  $\text{Pe}=5$  and the numerical domain size in the  $x$  direction is  $L/(2b)=128$ .

## B. Numerical methods

The three-dimensional partial differential equation for  $c$  given by Eq. (1) was solved in a rectangular box of size  $2b \times 2b \times L$ . At each time step, the boundary condition Eq. (1b) was used to couple the  $c$  calculation from Eq. (1) to the  $s$  calculation from Eq. (30). The  $s$  calculation used explicit Runge Kutta 4 (RK4) time stepping.<sup>38</sup> An unconditionally stable implicit time integration scheme (Crank Nicholson method) and spatial discretization, both of second order numerical accuracy,<sup>47</sup> were used for advancing the  $c$  field. The numerical grid size used was  $\Delta x = \Delta y = \Delta z = 0.033$  for problems A and B and  $0.5\Delta x = \Delta y = \Delta z = 0.05$  for problem C. In all cases  $dt=0.01$ . The finite axial length  $L$  of the numerical domain was chosen large enough so that  $|c(x=0)|$  and  $|c(x=L)|$  remained essentially zero (not larger than  $10^{-10}$ ) at all times. A zero total flux (sum of diffusive and convective components) boundary condition was applied at the ends of the channel. For solution to the flow field in problem C, the SIMPLER algorithm<sup>48</sup> was used (see Refs. 39 and 49 for details). The shape functions  $f$  and  $g$  and the quantities  $\beta$ ,  $\gamma$ , and  $\bar{f}_w$  for the trapezoidal cross section listed in Table I were calculated using a commercially available package (Matlab PDE Toolbox) employing the finite element method.<sup>47</sup> For solving the asymptotically reduced one-dimensional problem, RK4 time stepping and eighth order compact finite differences were used, similar to that in Ref. 7. A typical ratio of run times on a 2 GHz-512 Mbyte computer for the one-dimensional effective problem and the three-dimensional problem was of the order of  $10^{-2}$ . This considerable runtime economy is a practical benefit of the asymptotically reduced model developed here.

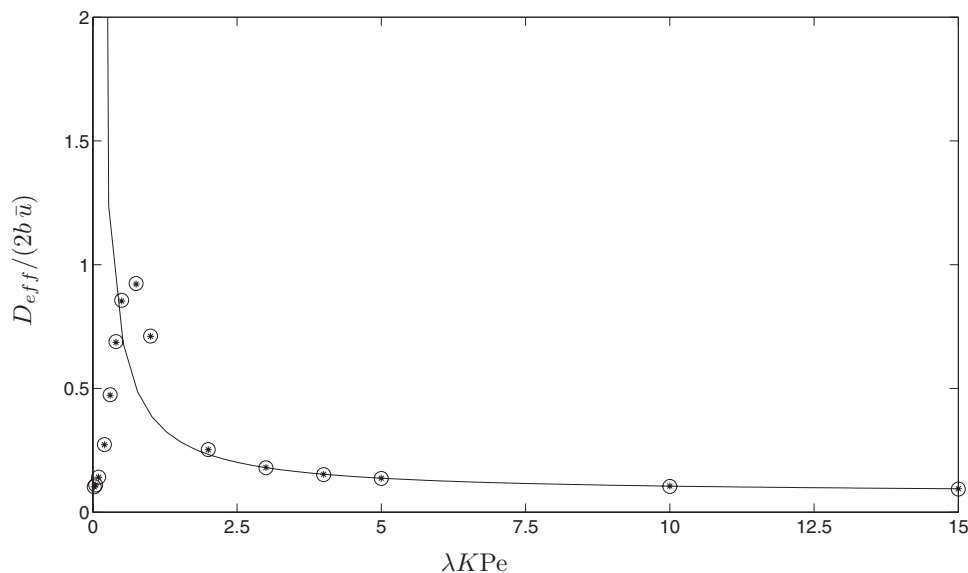


FIG. 3. Effective dispersion coefficient ( $D_{\text{eff}}$ ) at time  $t\bar{u}/(2b)=8$  vs adsorption rate constant ( $\lambda K Pe$ ) for problem A. Results from the three-dimensional numerical simulation are represented by asterisks and results from the simulation of the asymptotically reduced model are represented by circular symbols. The solid line is the effective dispersion coefficient  $D_{\text{eff}}^{(\text{chrom})}$  calculated from the theory of chromatography using Eq. (41). Here,  $Pe=10$ ,  $K=1$ , and  $L=80b$ .

### C. Results

In the results to be described below, an effective dispersion coefficient  $D_{\text{eff}}$  is used as a measure of the instantaneous rate of spreading of the solute in the axial direction. It is defined as follows:

$$D_{\text{eff}} = \frac{1}{2} \frac{d\sigma^2}{dt}, \quad (42)$$

where the variance of the plug is defined as  $\sigma^2 = \langle (x-x_*)^2 \bar{c} \rangle / \langle \bar{c} \rangle$  and  $x_*$  is the position of the centroid of the distribution,  $x_* = \langle x \bar{c} \rangle / \langle \bar{c} \rangle$ . In the above equation and henceforth,  $\langle \dots \rangle$  indicates axial average. Note, that in general  $D_{\text{eff}}$  evaluated from Eq. (42) is a time dependent quantity. The figures in this section use dimensionless variables. In particular, the concentration  $c$  is rendered dimensionless by dividing by the characteristic value  $c_0 = 1/(2b)^3 \int c(x,y,z,t=0) dV$  where the volume integral is over the entire computational domain.

#### 1. Problem A: EOF with wall reaction and infinitely thin Debye layers

The three-dimensional model for problem A involves solving Eq. (1) together with Eq. (30) and the one-dimensional model requires solving Eqs. (31) and (32). For the current problem,  $\beta = \gamma = 0$ , the function  $g=0$  everywhere and  $f = (6y^2 + 6z^2 - 1)/24$ . Therefore,  $\bar{f}_w = 1/24$  (as noted in Table I for square cross section). If only small departures from local equilibrium between the suspended and adsorbed phase is assumed, Eq. (41) may be used to calculate the effective dispersion. Though the parameter  $\lambda$  alone is varied, results are presented in terms of the combination  $\lambda K Pe$  representing a ratio of the characteristic adsorption time to the characteristic diffusion time. Figure 2 shows the time evolution of  $D_{\text{eff}}$  calculated from the asymptotically reduced equations and the full three-dimensional equations for

$\lambda K Pe = 1, 3, 5, 10$  with  $K=1$  and  $Pe=10$  held fixed. The two sets of computational results are in excellent agreement. Qualitatively,  $D_{\text{eff}}$  approaches a steady value after going through a transient phase. The transient phase is the most prolonged for  $\lambda K Pe = 1$ , because, slow reactions take a longer time to achieve the quasiequilibrium characteristic of chromatography. The asymptotically reduced model accurately represents the transient as well as the final equilibrium state for all four reaction speeds studied, whereas, the analytical estimate  $D_{\text{eff}}^{(\text{chrom})}$  in Eq. (41) can only be used to estimate the steady value. This is evident in Fig. 3 which shows the effect of varying  $\lambda K Pe$  on  $D_{\text{eff}}$  at a fixed time  $t\bar{u}/2b = 8$  predicted by the three-dimensional calculation, asymptotically reduced model and the analytical formula Eq. (41). The solid line shows  $D_{\text{eff}}^{(\text{chrom})}$  calculated by Eq. (41). It agrees with the full three-dimensional calculation only for large enough  $\lambda K Pe$ . But as the wall reaction rate gets slower,  $D_{\text{eff}}^{(\text{chrom})}$  diverges from the  $D_{\text{eff}}$  calculated from the three-dimensional simulation, because at  $t\bar{u}/2b = 8$ , equilibrium has not yet been reached. The one-dimensional model on the other hand is accurate even for slow reaction rates.

Figure 4 shows the solute distribution at  $t\bar{u}/2b = 28$  for  $\lambda K Pe = 1$  in the liquid phase  $\bar{c}$  (top pane) and solid phase  $\bar{s}$  (center pane) averaged at each cross section of the channel. The predictions of the asymptotically reduced model (solid line) and the three-dimensional model are in good agreement. The  $\bar{c}$  distribution has a positive skewness, as has been predicted elsewhere in the literature.<sup>27</sup> The bottom pane shows that the asymptotically reduced model can be used to calculate the solute distribution on cross-sectional planes, in good agreement with the three-dimensional model.

Figure 5 shows an interesting phenomenon in the transient phase for  $\lambda K Pe = 1$ , where a ‘‘lump’’ in the  $\bar{c}$  distribution forms due to pile up of desorbed material and grows progressively in mass to overwhelm the erstwhile primary peak upstream. Before this event the  $\bar{c}$  distribution is tailed

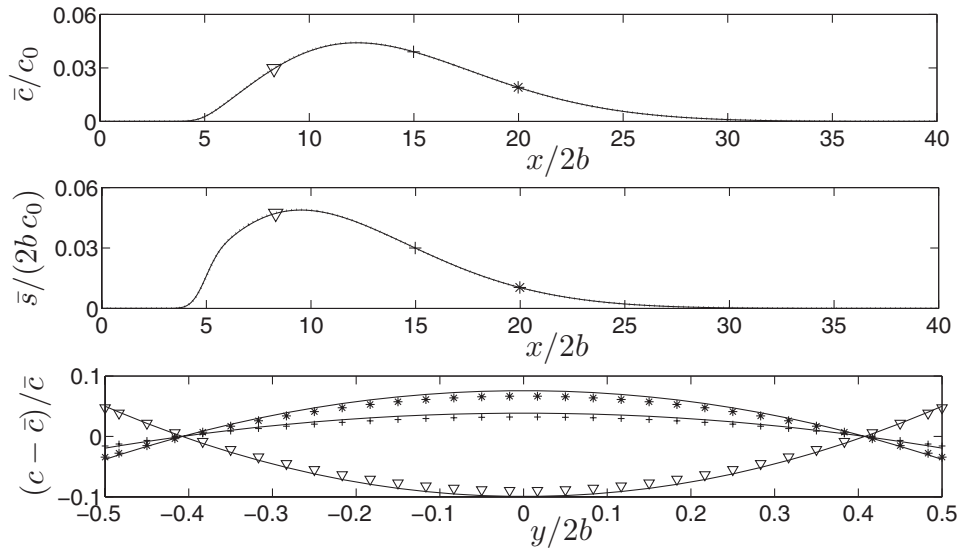


FIG. 4. The top pane shows the cross-sectionally averaged concentration ( $\bar{c}$ ) at time  $t\bar{u}/(2b)=28$  calculated for problem A with the three-dimensional model (dotted line) and asymptotically reduced model (solid line). The center pane shows the corresponding perimetrically averaged adsorbed concentration calculated using the three-dimensional model (dotted line) and asymptotically reduced model (solid line). In the top and middle panes the  $\bar{c}$  and  $\bar{s}$  values at cross-sectional planes at  $x/2b=8.33, 15, 20$  are represented by the symbols  $\nabla$ ,  $+$ ,  $*$ , respectively. In the bottom pane the corresponding centerline concentration distribution is shown for the three marked planes calculated using the three-dimensional model (symbols  $\nabla$ ,  $+$ ,  $*$ , respectively) and the asymptotically reduced model (solid lines). Here,  $Pe=10$ ,  $K=1$ ,  $\lambda K Pe=1$  and  $L=80b$ .

(negative skewness) and after this event the distribution is fronted (positive skewness). The inset shows this effect on the peak motion. The jump corresponding to the formation of the new peak is accurately resolved by the asymptotically reduced model.

## 2. Problem B: EOF with finite Debye layers

When the ratio  $\mathcal{K}=2b/\lambda_D$  can be considered to be infinitely large, we have a uniform EOF in an axially invariant channel. However, if the channel width is small enough for  $\mathcal{K}$  to be considered finite, the EOF is nonuniform across the cross section and gets progressively more nonuniform as  $\mathcal{K}$

is decreased. The flow distribution  $u(y,z)$  for noninfinitesimal  $\mathcal{K}$  can be calculated from the equilibrium potential  $\phi$ ,<sup>50</sup>

$$u = 1 - \phi, \quad (43)$$

where  $\phi$  is measured in units of the wall  $\zeta$  potential and  $u$  is measured in units of the slip velocity  $u_e$ . The potential  $\phi$  obtained by solving the Poisson-Boltzmann equation with the Debye-Hückel approximation<sup>8</sup> in a square cross section of side  $2b$  with specified zeta potential on all four walls is as follows:<sup>10</sup>

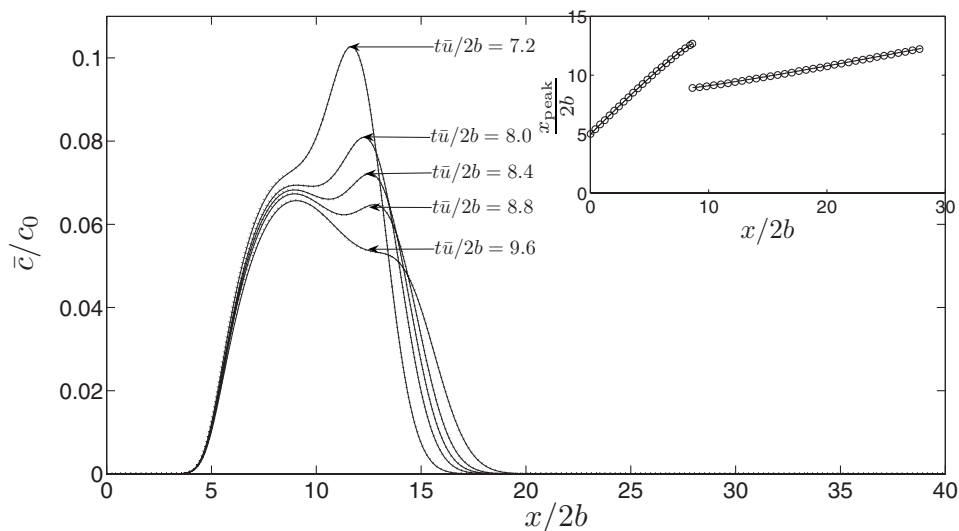


FIG. 5. Formation of a secondary peak in problem A for  $K=1$  and  $\lambda K Pe=1$  shown by plotting concentration distributions at times  $t\bar{u}/(2b) = 7.2, 8, 8.4, 8.8, 9.6$ . The dotted lines represent results from the three-dimensional model and the solid lines represent results from the asymptotically reduced model. The inset shows the variation in position of the solute concentration peak ( $x_{peak}$ ) with time. In the inset, circular symbols represent results from the three-dimensional solution and the solid line represents results from the asymptotic model.

TABLE II. Dependence of the coefficients  $\gamma$  and  $\beta$  on Debye layer thickness in problem B.

$2b/\lambda_D$	$\gamma$	$\beta$
4	0.0067	0.0140
8	0.0042	0.0115
12	0.0026	0.00932
16	0.0017	0.00772
20	0.0012	0.00655
24	0.0009	0.00568
28	0.00067	0.00500
32	0.00053	0.00447
36	0.00043	0.00403

$$\phi = 4 \left( \sum_{n=0}^{\infty} (-1)^n \left\{ \frac{\cos[(2n+1)\pi y] \cosh[\alpha_n z]}{(2n+1)\pi \cosh\left[\frac{\alpha_n}{2}\right]} + \frac{\cosh[(2n+1)\pi z] \cos[\alpha_n y]}{(2n+1)\pi \cosh\left[\frac{\alpha_n}{2}\right]} \right\} \right), \quad (44)$$

where  $\alpha_n = \sqrt{\mathcal{K}^2 + [(2n+1)\pi]^2}$ . In Eq. (44),  $y$  and  $z$  are measured from the center of the channel in units of  $2b$ .

The effect of decreasing  $\mathcal{K}$  (which can be achieved for example by using channels of progressively smaller widths) on solute transport in the presence of adsorption-desorption is to enhance dispersion through the Taylor-Aris dispersion mechanism, provided the mean flow in the channel is kept constant. Using the flow field  $u(y, z)$  from Eqs. (43) and (44), Eq. (25) can be solved and the coefficients  $\beta$  and  $\gamma$  can be calculated. An analytical solution of Eq. (25) in this case is possible but complicated, so numerical solution was resorted to. The values of  $\gamma$  and  $\beta$  required by the asymptotically reduced model for the values of  $\mathcal{K}$  under consideration are

tabulated in Table II. As in problem A,  $f$  is determined by geometry and the coefficient  $\bar{f}_w = 1/24$  is independent of  $\mathcal{K}$ .

Figure 6 shows the effective dispersion coefficient calculated at time  $t\bar{u}/2b = 7.75$  for the values of  $\mathcal{K}$  reported in the first column of Table II. Here, the mean flow is held constant across all values of  $\mathcal{K}$ ; thus the flow profile changes only in shape on changing  $\mathcal{K}$ . The results calculated with three-dimensional simulation and the reduced asymptotic model are in good agreement. In addition, in Fig. 6, we have calculated the effective dispersion coefficient when  $\mathcal{K} \rightarrow 0$  and when  $\mathcal{K} \rightarrow \infty$ , utilizing the fact that the electrokinetic flow calculated by the Debye-Hückel approximation approaches the same description as a pressure-driven flow and a uniform flow, respectively, in these two limits.

### 3. Problem C: EOF with variable $\zeta$ potentials

The mean flow rate in this problem can be calculated by  $\bar{u} = -\langle \zeta \rangle$ .<sup>42</sup> The distribution of the axial flow component is necessary in the right-hand side of Eq. (25a) to calculate  $g$  for the asymptotically reduced model. Using the lubrication approximation<sup>42</sup> for flow (which is expected to be strictly accurate for  $2b/\Lambda \ll 1$ ), we get

$$\frac{u}{\bar{u}} - 1 = \left( 1 - \frac{\zeta}{\langle \zeta \rangle} \right) \left( \frac{u_p}{\bar{u}_p} - 1 \right). \quad (45)$$

The quantities  $u_p$  and its cross-sectional average  $\bar{u}_p$  are defined in Ref. 42 and calculated for rectangular cross sections in Ref. 39. The combination  $u_p/\bar{u}_p$  represents the flow profile of a fully developed pressure-driven flow of unit flow rate. Using  $\gamma$  and  $\bar{g}_w = \beta$  from Table I, we get  $\gamma \bar{u}^2 = 0.0084(\langle \zeta \rangle - \zeta)^2$  and  $\bar{g}_w \bar{u} = 0.0155(\langle \zeta \rangle - \zeta)$  for use in Eqs. (32) and (31), respectively.

The variation of the effective dispersion coefficient with time is plotted for the wavelengths  $\Lambda = L/5 = 51.2b$ ,  $\Lambda = L/10 = 25.6b$ , and  $\Lambda = L/25 = 10.24b$  in the three panes of Fig. 7, when the amplitude  $\Delta\zeta = 0.75\zeta_0$  is fixed. The predic-

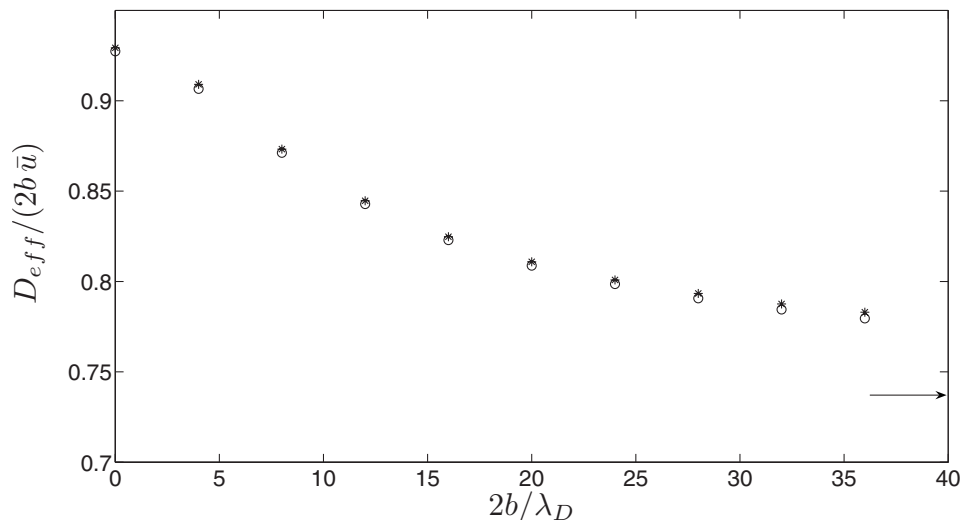


FIG. 6. Effect of the fraction of channel width occupied by the Debye layer ( $2b/\lambda_D$ ) on the effective dispersion coefficient  $D_{\text{eff}}$  calculated for problem B from three-dimensional numerical simulation (asterisks) and simulation of asymptotically reduced model (circular symbols). The effective dispersion coefficient in the infinitely thin Debye layer limit is calculated using uniform flow and indicated by the arrow mark in the figure.

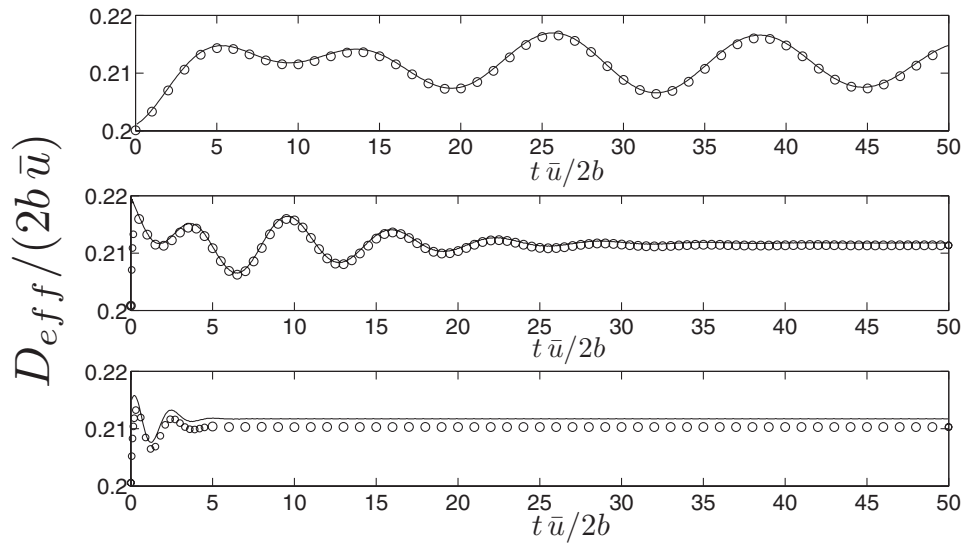


FIG. 7. Effective dispersion coefficient ( $D_{\text{eff}}$ ) vs time,  $t\bar{u}/(2b)$ , for axially variable zeta potential of wavelength  $\Lambda$  (problem C) calculated from the three-dimensional numerical simulation (solid line) and the simulation of the one-dimensional model (circular symbols). Parameters are (top, center, and bottom panes, respectively)  $\Lambda=L/5=51.2b$ ,  $\Lambda=L/10=25.6b$ , and  $\Lambda=L/25=10.24b$ , in all cases,  $\Delta\zeta/\zeta_0=0.75$ .

tions of the asymptotically reduced model for the wavelengths  $\Lambda=L/5=51.2b$  and  $\Lambda=L/10=25.6b$  are reasonably accurate. For  $\Lambda=L/25=10.24b$ , some inaccuracies are visible. This is because the assumption of slow spatial variation used for the asymptotic reduction of the concentration field and the lubrication approximation of the flow field<sup>42</sup> is inappropriate for short wavelength perturbations. If the elapsed time is long enough for the characteristic width of the  $\bar{c}$  distribution to significantly exceed a half wavelength of the wall zeta potential perturbation, the effective dispersion coefficient achieves a stationary value, as in the center and bottom panes. The three-dimensional solution for  $\Lambda=L/10$  and  $\Lambda=L/25$  in Fig. 7 show a short transient period corresponding to cross-diffusion, for which asymptotic results are inaccurate.

The effect of varying  $\Delta\zeta$  on  $D_{\text{eff}}$  is shown in Fig. 8. A higher perturbation in the electro-osmotic flow produces higher dispersion, since  $\gamma\bar{u}^2=0.0084(\langle\zeta\rangle-\zeta)^2$ . The predictions of the asymptotically reduced model are in good agreement with the three-dimensional results.

Figure 9 shows the applied zeta potential in the top pane and the solute distribution  $\bar{c}$  at  $t\bar{u}/2b=15$  in the center pane. The wavelength  $\Lambda=L/5=51.2b$ . The mean concentration calculated using the asymptotically reduced model agrees well with the calculation based on the three-dimensional model. The bottom pane shows that the asymptotically reduced model can be used to obtain the solute distribution at each cross section. The cross-sectional distributions at three axial locations are calculated by direct simulation in the

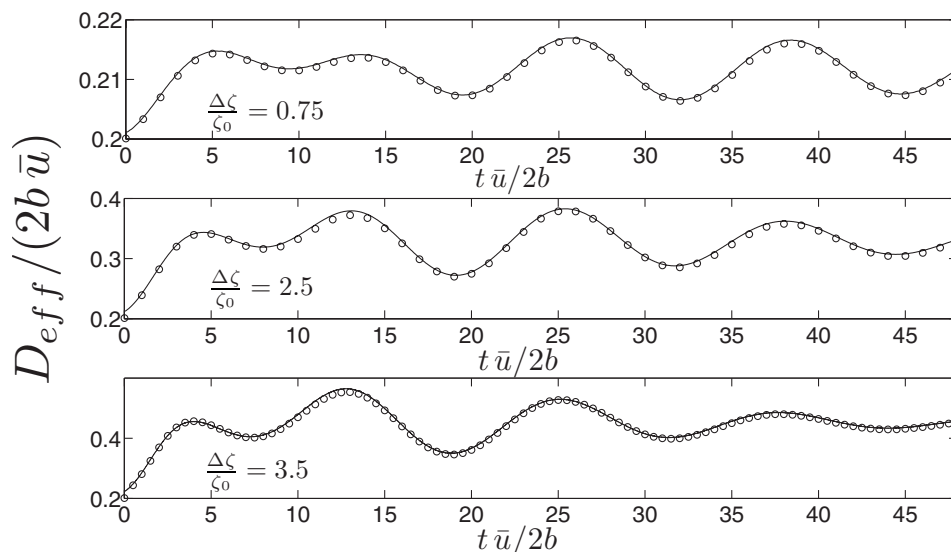


FIG. 8. Effective dispersion coefficient ( $D_{\text{eff}}$ ) vs time,  $t\bar{u}/(2b)$ , for axially variable zeta potential (problem C) with three different wave amplitude values  $\Delta\zeta/\zeta_0=0.75, 2.5, 3.5$  (top, center, and bottom panes, respectively). Calculation based on the three-dimensional numerical simulation (circular symbols) is compared to a simulation of the one-dimensional model (solid line). Here  $\Lambda=L/5=51.2b$ .

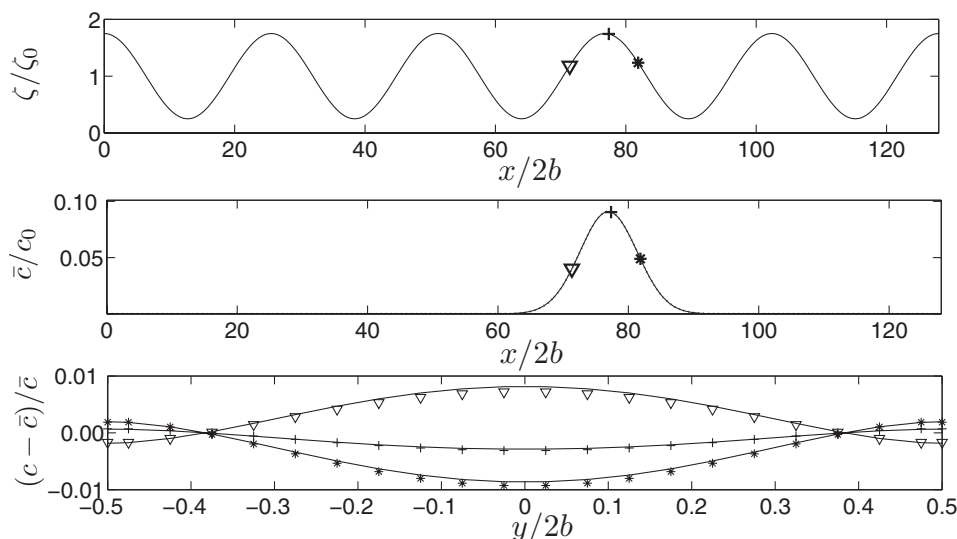


FIG. 9. An applied zeta potential distribution in problem C of wavelength  $\Lambda=L/5=51.2b$  and amplitude  $\Delta\zeta/\zeta_0=0.75$  (top pane). The symbols  $\nabla$ ,  $+$ , and  $*$  mark three interrogation planes along the channel. The center pane shows the cross-sectionally averaged concentration at time  $t\bar{u}/(2b)=15$  calculated with the asymptotically reduced model (solid line) and three-dimensional model (dotted line). The bottom pane shows the centerline concentration profiles at the three interrogation planes calculated from the three-dimensional simulation (symbols  $\nabla$ ,  $+$ ,  $*$ , respectively) and the asymptotically reduced model (solid lines). Here  $\Lambda=L/5=51.2b$  and  $\Delta\zeta/\zeta_0=0.75$ .

three-dimensional model and by use of Eq. (23) in the asymptotically reduced model. The two are in good agreement.

## V. CONCLUSIONS

The problem of transport of a solute in an axially variable flow and cross-sectional geometry in the presence of adsorption and desorption on the walls of the channel has been studied with an asymptotic method that leads to a reduced system of one-dimensional partial differential equations. The results from the asymptotic reduction are expected to be accurate for transport and wall interactions in microchannels used for separations like CE and CEC, after a short transient phase at the beginning of the analysis of the order of cross-channel diffusion time, provided any explicit axial variation (such as that of wall zeta potential and cross-sectional shape) has a scale large compared to the channel width and any explicit temporal variation (such as that of AC voltages used for flow generation, as in Ref. 46) has a large scale compared to the cross-channel diffusion time.

The main results of the asymptotic analysis are the coupled partial differential Eqs. (27) and (29) and Eq. (23) for calculating variation of concentration across the microchannel. These equations require only one-dimensional numerical solution, which is computationally much less expensive than the three-dimensional solution required by the complete problem of transport and wall reaction.

The effect of cross-sectional shape and a background flow which may or may not vary axially is incorporated in a simple manner in the asymptotically reduced model through the calculation of “shape functions.” The analysis can be applied to both slow and fast wall interactions, unlike results from the theory of chromatography,<sup>25</sup> which emerge as a special case of the model when the adsorption and desorption on the wall are fast enough to reach a state of “quasiequilibrium” within the time of analysis.

The asymptotically reduced model is applied to three test problems motivated by CE and CEC applications that include adsorption-desorption, axial flow variation, and electrokinetic effects characteristic of nanochannels. The results from solving the asymptotically reduced model are compared against those from the three-dimensional solution of the problem, achieved at a much higher computational cost. The one-dimensional results are found to be in very good agreement with the three-dimensional results, except in the situation when the scale of axial variation in the problem is comparable in scale to the channel width.

## ACKNOWLEDGMENTS

Support from the NSF under Grant No. CTS-0330604 is gratefully acknowledged. The authors are thankful to Dr. Neelesh A. Patankar for providing the computer code used for three-dimensional numerical solution of the transport equation.

## APPENDIX A: DERIVATION OF EQ. (17)

By the definition of derivative,

$$\left( \int_{\Omega} F dA \right)_X = \lim_{\Delta X \rightarrow 0} \frac{\int_{\Omega(X+\Delta X)} F(X+\Delta X) dA - \int_{\Omega(X)} F(X) dA}{\Delta X}. \quad (\text{A1})$$

The first integral in Eq. (A1) can be split into

$$\begin{aligned} \int_{\Omega(X+\Delta X)} F(X+\Delta X) dA &= \int_{\Omega(X)} F(X+\Delta X) dA \\ &+ \int_{[\Omega(X+\Delta X)-\Omega(X)]} F(X+\Delta X) dA. \end{aligned} \quad (\text{A2})$$

The domain of integration  $[\Omega(X+\Delta X)-\Omega(X)]$  for the second

integral above is a thin annulus on the  $\Omega(X+\Delta X)$  plane, is shown in Fig. 1. The differential area element of this annulus is  $-dXdS$ , if the channel cross section varies slowly. Therefore,

$$\begin{aligned} & \int_{[\Omega(X+\Delta X)-\Omega(X)]} F(X+\Delta X)dA \\ &= \Delta X \oint_{\partial\Omega} F(X)ldS + O(\Delta X)^2. \end{aligned} \quad (\text{A3})$$

Using Eq. (A3) in Eq. (A2) and the result in Eq. (A1) we get

$$\left( \int_{\Omega} FdA \right)_X = \int_{\Omega} F_X dA - \oint_{\partial\Omega} FldS \quad (\text{A4})$$

after utilizing the definition of the derivative of the function  $F(X)$  in variable  $X$ .

## APPENDIX B: DERIVATION OF $\bar{g}_w = \beta$

In the left-hand side of the mathematical identity,

$$\int (\mathbf{f}\nabla_{\Omega}^2 g - g\nabla_{\Omega}^2 f)dA = \oint (\mathbf{f}\nabla_{\Omega} g \cdot \hat{\mathbf{n}}_{\Omega} - g\nabla_{\Omega} f \cdot \hat{\mathbf{n}}_{\Omega})dS \quad (\text{B1})$$

we use Eqs. (24a), (24c), (25a), and (25c); this simplifies the left-hand side to  $\int fu/\bar{u}dA$ .

For simplifying the first term in the right-hand side of Eq. (B1), the right-hand of side of Eq. (24b) [which is required to be only  $O(1)$  accurate, by virtue of Eq. (13b)] can be replaced by  $1/\alpha$ . This is because,  $s = \bar{s} + O(1)$  provided the kinetic coefficients and the initial distribution of  $s$  do not vary on  $\partial\Omega$ . Indeed, the evolution equation for  $s$ ,  $s_t = h(\bar{c}, s) + O(\epsilon)$  ensures that if  $s = \bar{s} + O(\epsilon)$  at  $t=0$ , it will remain so at future times.

The second term on the right-hand side is zero owing to Eq. (25b). Utilizing the definition of  $\beta$  by Eq. (26a) and  $\alpha = P/A$ , we get

$$\beta = \frac{1}{A} \int f \frac{u}{\bar{u}} dA = \frac{1}{P} \oint g dS = \bar{g}_w. \quad (\text{B2})$$

<sup>1</sup>H. A. Stone, A. D. Stroock, and A. Ajdari, "Engineering flows in small devices: Microfluidics toward a lab-on-a-chip," *Annu. Rev. Fluid Mech.* **36**, 381 (2004).

<sup>2</sup>J. A. Wilkins and C. Horváth, "Capillary electrochromatography of peptides and proteins," *Electrophoresis* **25**, 2242 (2004).

<sup>3</sup>*Electrokinetic Phenomena: Principles and Applications in Analytical Chemistry and Microchip Technology*, edited by A. S. Rathore and A. Guttman (Marcell Dekker, New York, 2004).

<sup>4</sup>M. Pačes, J. Kosek, M. Marek, U. Tallarek, and A. Seidel-Morgenstern, "Mathematical modelling of adsorption and transport processes in capillary electrochromatography: Open-tubular geometry," *Electrophoresis* **24**, 380 (2003).

<sup>5</sup>J. K. Towns and F. E. Regnier, "Impact of polycation adsorption on efficiency and electro-osmotically driven transport in capillary electrophoresis," *Anal. Chem.* **64**, 2473 (1992).

<sup>6</sup>M. R. Schure and A. M. Lenhoff, "Consequences of wall adsorption in capillary electrophoresis: Theory and simulation," *Anal. Chem.* **65**, 3024 (1993).

<sup>7</sup>S. Ghosal, "The effect of wall interactions on capillary zone electrophoresis," *J. Fluid Mech.* **491**, 285 (2003).

<sup>8</sup>R. Probstein, *Physicochemical Hydrodynamics* (Wiley, New York, 1994).

<sup>9</sup>S. Ghosal, "Electrokinetic flow and dispersion in capillary electrophoresis," *Annu. Rev. Fluid Mech.* **38**, 309 (2006).

<sup>10</sup>C. Yang and D. Li, "Analysis of electrokinetic effects on the liquid flow in rectangular microchannels," *Colloids Surf., A* **143**, 339 (1998).

<sup>11</sup>G. I. Taylor, "Dispersion of soluble matter in solvent flowing slowly through a tube," *Proc. R. Soc. London, Ser. A* **219**, 186 (1953).

<sup>12</sup>R. Aris, "On the dispersion of a solute in a fluid flowing through a tube," *Proc. R. Soc. London, Ser. A* **235**, 67 (1956).

<sup>13</sup>S. Devasenathipathy, J. G. Santiago, and K. Takehara, "Particle tracking techniques for electrokinetic microchannel flows," *Anal. Chem.* **74**, 3704 (2002).

<sup>14</sup>A. Ajdari, "Electro-osmosis on inhomogeneously charged surfaces," *Phys. Rev. Lett.* **75**, 755 (1995).

<sup>15</sup>A. Ajdari, "Generation of transverse fluid currents and forces by an electric field: Electro-osmosis on charge-modulated and undulated surfaces," *Phys. Rev. E* **53**, 4996 (1996).

<sup>16</sup>J. K. Towns and F. E. Regnier, "Capillary electrophoretic separations of proteins using nonionic surfactant coatings," *Anal. Chem.* **91**, 1126 (1992).

<sup>17</sup>M. S. Munson, M. S. Hasenbank, E. Fu, and P. Yager, "Suppression of nonspecific adsorption using sheath flow," *Lab Chip* **4**, 438 (2004).

<sup>18</sup>S. C. Jacobson, R. Hergenroeder, L. B. Koutny, and J. M. Ramsey, "Open channel electrochromatography on a microchip," *Anal. Chem.* **66**, 2369 (1994).

<sup>19</sup>J. H. Knox, "Thermal effects and band spreading in capillary electro-separation," *Chromatographia* **26**, 329 (1988).

<sup>20</sup>U. Tallarek, E. Rapp, T. Scheenen, E. Bayer, and H. Van As, "Electroosmotic and pressure-driven flow in open and packed capillaries: Velocity distributions and fluid dispersion," *Anal. Chem.* **72**, 2292 (2000).

<sup>21</sup>M. C. Breadmore, M. Boyce, M. Macka, N. Avdalovic, and P. R. Haddad, "Peak shapes in open tubular ion-exchange capillary electrochromatography of inorganic anions," *J. Chromatogr., A* **892**, 303 (2000).

<sup>22</sup>K. Shariff and S. Ghosal, "Peak tailing in electrophoresis due to alteration of the wall charge by adsorbed analytes: Numerical simulations and asymptotic theory," *Anal. Chim. Acta* **507**, 87 (2003).

<sup>23</sup>S. Ghosal, "Fluid mechanics of electro-osmotic flow and its effect on band broadening in capillary electrophoresis," *Electrophoresis* **25**, 214 (2004).

<sup>24</sup>M. J. E. Golay, "Theory of chromatography in open and coated tubular columns with round and rectangular cross sections," in *Gas Chromatography 1958: Proceedings of the Second Symposium*, Amsterdam, May 19–23, 1958, edited by D. H. Desty (Butterworths Scientific, London, 1958), pp. 36–45.

<sup>25</sup>J. C. Giddings, *Dynamics of Chromatography, Part I, Principles and Theory* (Marcel Dekker, New York, 1965).

<sup>26</sup>R. Aris, "On the dispersion of a solute by diffusion, convection and exchange between phases," *Proc. R. Soc. London, Ser. A* **252**, 538 (1959).

<sup>27</sup>J. C. Giddings, "Generation of variance, "theoretical plates," resolution, and peak capacity in electrophoresis and sedimentation," *Sep. Sci.* **4**, 181 (1969).

<sup>28</sup>J. R. Conder and C. L. Young, *Physicochemical Measurement by Gas Chromatography* (Wiley, Chichester, 1979).

<sup>29</sup>L. R. Snyder and J. J. Kirkland, *Introduction to Modern Liquid Chromatography* (Wiley, New York, 1979).

<sup>30</sup>B. Verzola, C. Gelfi, and P. G. Righetti, "Protein adsorption to the bare silica wall in capillary electrophoresis quantitative study on the chemical composition of the background electrolyte for minimizing the phenomenon," *J. Chromatogr., A* **868**, 85 (2000).

<sup>31</sup>A. T. Conlisk, J. McFerran, Z. Zheng, and D. Hansford, "Mass transfer and flow in electrically charged micro- and nanochannels," *Anal. Chem.* **74**, 2139 (2002).

<sup>32</sup>G. Desmet and G. V. Baron, "On the possibility of shear-driven chromatography: a theoretical performance analysis," *J. Chromatogr., A* **855**, 57 (1999).

<sup>33</sup>S. Debesset, C. J. Hayden, C. Dalton, J. C. T. Eijkel, and A. Manz, "An ac electro-osmotic micropump for circular chromatographic applications," *Lab Chip* **4**, 396 (2004).

<sup>34</sup>H. Brenner and D. A. Edwards, *Macrotransport Processes* (Butterworth-Heinemann, Boston, 1993).

<sup>35</sup>R. Sankarasubramanian and W. N. Gill, "Unsteady convective diffusion with interphase mass transfer," *Proc. R. Soc. London, Ser. A* **333**, 115 (1973).

<sup>36</sup>E. M. Lungu and H. K. Moffatt, "The effect of wall conductance on heat diffusion in duct flow," *J. Eng. Math.* **16**, 121 (1982).

- <sup>37</sup>G. N. Mercer and A. J. Roberts, "A centre manifold description of contaminant dispersion in channels with varying flow properties," *SIAM J. Appl. Math.* **50**, 1547 (1990).
- <sup>38</sup>G. Dahlquist, *Numerical Methods* (Courier Dover, New York, 2003), pp. 349.
- <sup>39</sup>S. Datta, S. Ghosal, and N. A. Patankar, "Electro-osmotic flow in a rectangular channel with variable wall zeta-potential: Comparison of numerical simulation with asymptotic theory," *Electrophoresis* **27**, 611 (2006).
- <sup>40</sup>D. Dutta and D. T. Leighton, "A low dispersion geometry for microchip separation devices," *Anal. Chem.* **74**, 1007 (2002).
- <sup>41</sup>The factor  $\sqrt{1-\epsilon^2\ell^2}$  was missed in Ref. 42, though the final equations are unaffected since the correction does not have contributions at the level of lubrication theory.
- <sup>42</sup>S. Ghosal, "Lubrication theory for electro-osmotic flow in a channel of slowly varying cross-section and wall charge," *J. Fluid Mech.* **459**, 103 (2002).
- <sup>43</sup>M. R. Doshi, P. M. Daiya, and W. N. Gill, "Three dimensional laminar dispersion in open and closed rectangular conduits," *Chem. Eng. Sci.* **33**, 795 (1978).
- <sup>44</sup>P. C. Chatwin and P. J. Sullivan, "The effect of aspect ratio on longitudinal diffusivity in rectangular channels," *J. Fluid Mech.* **120**, 347 (2006).
- <sup>45</sup>R. Datta and V. R. Kotamarthi, "Electrokinetic dispersion in capillary electrophoresis," *AIChE J.* **36**, 916 (1990).
- <sup>46</sup>A. Ajdari, "Electrokinetic 'ratchet' pumps for microfluidics," *Appl. Phys. A: Mater. Sci. Process.* **75**, 271 (2002).
- <sup>47</sup>J. H. Ferziger and M. Peric, *Computational Methods for Fluid Dynamics* (Springer, New York, 2002).
- <sup>48</sup>S. V. Patankar, *Numerical Heat Transfer and Fluid Flow* (Hemisphere, Washington, 1980), p. 126.
- <sup>49</sup>N. A. Patankar and H. H. Hu, "Numerical simulation of electro-osmotic flow," *Anal. Chem.* **70**, 1870 (1998).
- <sup>50</sup>B. J. Kirby and E. F. Hasselbrink, "Zeta potential of microfluidic substrates: 1. Theory, experimental techniques, and effects on separations," *Electrophoresis* **25**, 187 (2004).